Supporting Information

Triggering electronic microenvironment of extraordinary nitrogen-bridged atomic iron coordinated with in-plane nitrogen by manipulating phase-reconfigured 2D vanadium nitride MXene toward invigorated lithium-sulfur batteries

Xinlu Zhang,[a,b] Xuexiu Bai,[a] Chuanliang Wei,[b] ZhengRan Wang,[a] Baojuan Xi,[b] Shenglin Xiong,[b] and Jinkui Feng* [a,b]

[a.] Key Laboratory for Liquid-Solid Structural Evolution & Processing of Materials (Ministry of Education), Research Center for Carbon Nanomaterials, School of Materials Science and Engineering, Shandong University, Jinan 250061, P. R. China

[b.] Shenzhen Institute of Shandong University, Shenzhen 518057, P. R. China

* Corresponding author: Jinkui Feng

E-mail address: jinkui@sdu.edu.cn (J. Feng)

Experimental Section

Synthesis of $Fe_{N4\text{-}O\text{-}NC}$-VN: V_2GaN was added into 1-Butyl-3-methyl-1H-imidazol-3-ium tetrachloroferrate(III) solution that vigorously stirred at room temperature. The above-mentioned mixture were respectively transferred into quarts tubes that were heated to 450 and 550 ^oC with heating ramp of 2 ^oC min^{-1} for 48 h. After that, achieved black powders cooled down to room temperature were disperated in the 1 M HCl solution magnetically stirring for 12 h. Subsequently, mixture solution was filtrated and washed using deionized water by vacuum pump. Finally, achieved powders were dried under vacuum oven at 50 ^oC for overnight, and denoted as $V_2Ga_{1-x}N$ and $Fe_{N4\text{-}O\text{-}NC}$-VN.

Synthesis of $Fe_{N4\text{-}O}$-VN: V_2GaN powder was mixed and grounded with NaCl, KCl and $FeCl_3$ for 0.5 h. The mixture was heated to 550 ^oC with heating ramp of 2 ^oC min^{-1} for 48 h under the mixed gas of NH_3/argon atmosphere. Afterward, the obtiained powder were magnetically stirred in 1 M HCl solution for 12 h. Finally, the above-mentioned mixture solution was filtrated and washed using deionized water by vacuum pump to achieve $Fe_{N4\text{-}O}$-VN.

Synthesis of active electrodes: Active materials of $V_2Ga_{1-x}N$ or $Fe_{N4\text{-}O\text{-}NC}$-VN, Super P and poly(vinylidene fluoride)(PVDF) with weight ratio of 8:1:1 were grinded by N-methyl pyrrolidinone (NMP) to result in homogeneous slurry coated on Al foil. Subsequently, modified Al foil was dried under vacuum oven at 100 ^oC for overnight.

Synthesis of sulfur cathodes: Sublimed sulfur and Ketjen Black (KB) with mass ratio of 7:3 were grinded and transferred into quarz tubes that were heated to 155 ^oC for 10 h and continuely heated to 185 ^oC for 2 h with heating ramp of 3 ^oC min^{-1}, denoted as S/KB. The S/KB, Super P and PVDF with weight ratio of 7:2:1 were grinded by NMP as solvent to result in homogeneous slurry coated on Al foil. Finelly, the modified Al foil was dried under vacuum oven at 60 ^oC for overnight. The areal mass loading of sulfur cathode was 1.2-1.5 mg cm^{-2}.

Synthesis of different materials modified separators: The modified separators were synthesized by blade coating the homogeneous slurry of $V_2Ga_{1-x}N$ or $Fe_{N4\text{-}O\text{-}NC}$-VN, PVDF and Super P with mass ratio of 8:1:1 on commercial Celgard PP separator. After that, the separators were transferred into vacuum oven heated to 60 ^oC for overnnight. The achieved separators denoted as $V_2Ga_{1-x}N$@PP and $Fe_{N4\text{-}O\text{-}NC}$-VN@PP.

Synthesis of Li_2S_6 electrolyte: Sublimed sulfur and Li_2S with molar ratio of 5:1 were added into traditional electrolyte containing 1.0 M LiTFSI in 1,3-dioxolane/dimethyl ether (v/v=1:1) with 1.0 wt.% $LiNO_3$) magnetically stirred until yielding brownish-red Li_2S_6.

Li_2S_6 visialized adsorption test: Active materials ($V_2Ga_{1-x}N$ or $Fe_{N4\text{-}O\text{-}NC}$-VN) were respectively added into above-synthesized Li_2S_6 solution stood for 12 h. Additionally, blank Li_2S_6 solution was used as comparison.

Li_2S_6 penetration test: The above-synthesized Li_2S_6 solution and glycol dimethyl ether (DME) solvent with volum ratio of 1:1 were respectively tansferred into two sides of H-tube using pristine and modified separators

Redox kinetic test: Two identical active electrodes as working and referrence/counter electreodes were assembled into symmetric CR2032 coin cells with 0.25 M Li_2S_6 electrolyte in glox box filled Ar. The cyclic voltammetry (CV) tests of symmetric cell operate at potential range of -1.0-1.0 V to assess polysulfide redox kinetics.

Li_2S nucleation/decomposition: The above-synthesized active electrodes as cathode and lithium foil as referrence/counter electrode were assembled into CR2032 coin cells with 0.25 M Li_2S_6 electrolyte as catholyte and traditional electrolyte without Li_2S_6 as anolyte. For Li_2S nucleation, assembled cells were galvanostatically discharged to 2.08 V at 0.1 mA and subsequently potentiostatically discharged to 2.06 V for 10000 s. For Li_2S decomposition

experimental, assembled coin cell were galvanostatically discharged to 1.7 V at 0.1 mA and subsequently potentiostatically charged to 2.35 V for 10000 s.

Ex situ measurements: The assembled CR2032 coin cells were charged/discharged to given potentials disassembled in glove box filled with Ar. The obtained electrodes were naturally dried and stood in glove box untill to be investigated by PXRD and XPS.

Material characterization：The structure and morphology of these materials were respectively investigated by powder X-ray diffraction (PXRD, Rigaku Miniflex 600 X-ray Diffractometer), Raman (Renishaw Raman spectroscopy, Britain) with a 532 nm laser, Field Emission Scanning Electron Microscope (FESEM, JSM-7610F, Japan), Transmission electron microscopy (TEM, JEOL-2100F) and high-resolution transmission electron microscopy (HRTEM, JEOL-2100F), High-angle annular dark-field with spherical aberration-corrected transmission electron microscopy (HAADF-STEM) with Linköping's double Cs corrected FEI-Titan Cubed Themis G2 300 microscope, X-ray photoelectron spectra (XPS, Thermo Scientific K-Alpha), ultraviolet visualized spectra (UV-vis, Shimadzu, Japan), Nitrogen adsorption and desorption isotherm (Micromeritics ASAP2460, USA), Electron spin resonance (EPR, Bruker EMX PLUS), Inductively coupled plasma optical emission spectrometry (ICP-OES, Thermo Fisher iCAP PRO), ^{57}Fe Mössbauer spectra (ms500), Contact angle test (DSA100), X-ray absorption near-edge spectroscopy (XANES) and extended X-ray absorption fine spectroscopy (EXAFS) (Shanghai Synchrotron Radiation Facility, 200 mA, 3.0 GeV), Contact angles measurement (JY-82C).

Electrochemical Measurements: The CR2032 coin cells were assembled by sulfur cathode, lithium anode and different separators using traditional electrolyte of 1.0 M LiTFSI in 1,3-dioxolane/dimethyl ether (V/V=1:1) with 1.0 wt.% $LiNO_3$ in glove box filled with Ar. The symmetric cells were assembled by two idential electrodes of lithium foil or active electrode using specified electrolyt and separators in glove box filled with Ar. The CV curves and electrochemical impedance spectra (EIS) were performed on electrochemical workstation (CHI 660E, Chenhua, Shanghai), while electrochemical performances of different cells were investigated on Neware BTS system at different current densities.

Density Functional Theory: All preliminary calculations were conducted by utilizing first-principles simulations within the framework of density functional theory (DFT) employing Vienna Ab Initio Package (VASP),[1, 2] optimized by Perdew-Burke-Ernzerhof (PBE) functional derived from generalized gradient approximation (GGA) formulation.[3] The interactions of ionic cores and valence electrons were described by projected augmented wave (PAW) potentials by a plane wave basis set with a kinetic energy cutoff of 450 eV.[4, 5] Partial occupancies of

Kohn−Sham orbitals were simulated by using Gaussian smearing method and a width of 0.05 eV. When energy change was smaller than 10^{-5} eV, electronic energy was considered self-consistent, while a geometry optimization was considered convergent when force change was smaller than 0.05 eV/Å. The dispersion interactions were analysized by Grimme's DFT-D3 methodology.[6] In term of structural optimizations, gamma point in the Brillouin zone was used for k-point sampling. The free energy of a gas phase molecule or an adsorbate on surface was calculated by equation G = E + ZPE − TS, where E stands for total energy, ZPE represents zero-point energy, T denotes as temperature in kelvin (298.15 K), and S is entropy. The reported standard hydrogen electrode (SHE) model was employed by the calculations of Gibbs free energy changes (ΔG) of all reaction steps to evaluate the reaction barrier.

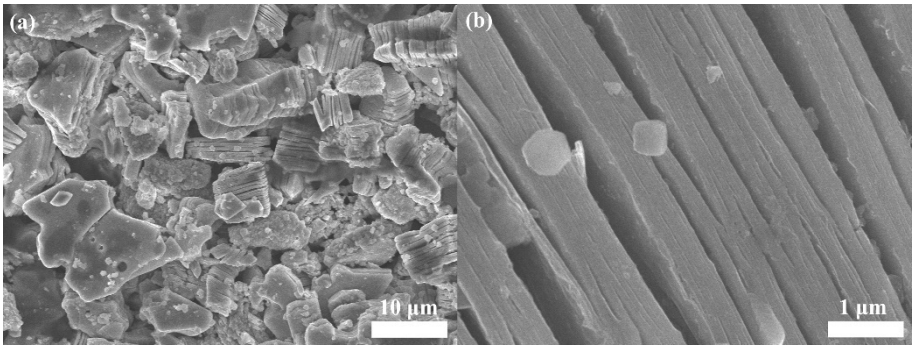

Fig. S1. SEM images of Fe_{N4-O}-VN.

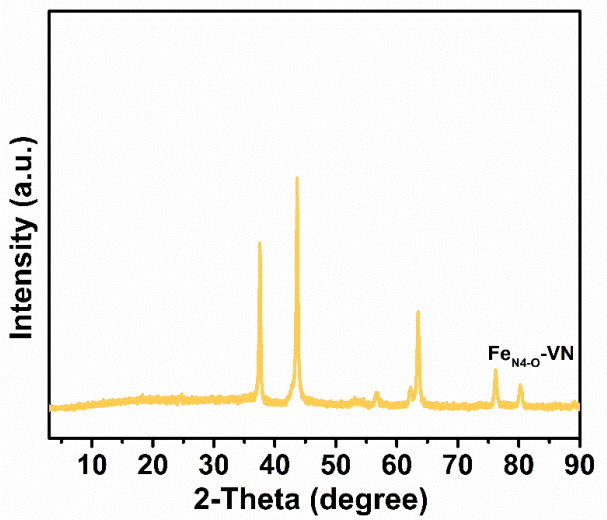

Fig. S2. PXRD pattern of Fe_{N4-O}-VN.

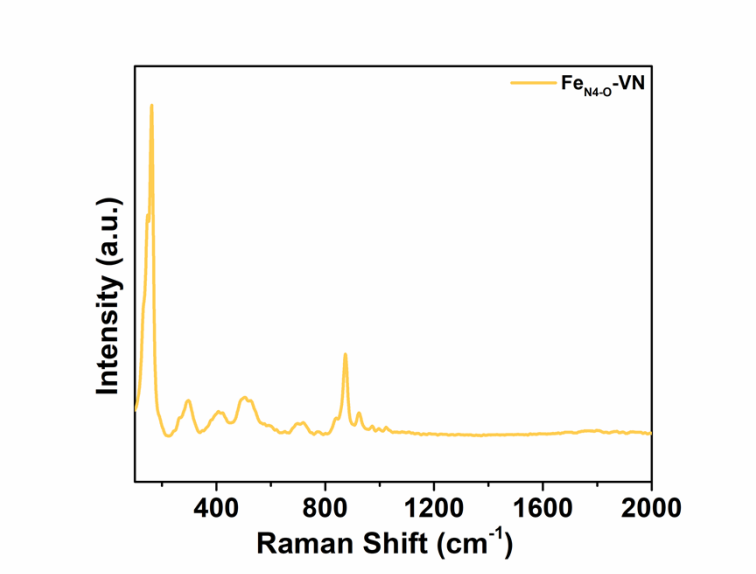

Fig. S3. Raman spectrum of Fe_{N4-O}-VN.

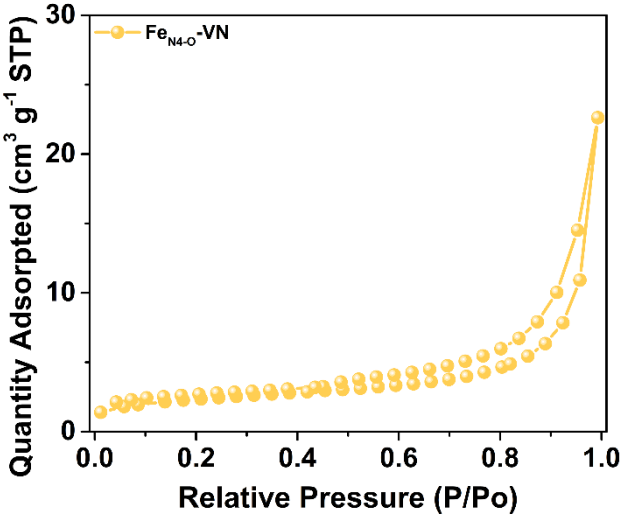

Fig. S4. Nitrogen adsorption/desorption isotherm of Fe_{N4-O}-VN.

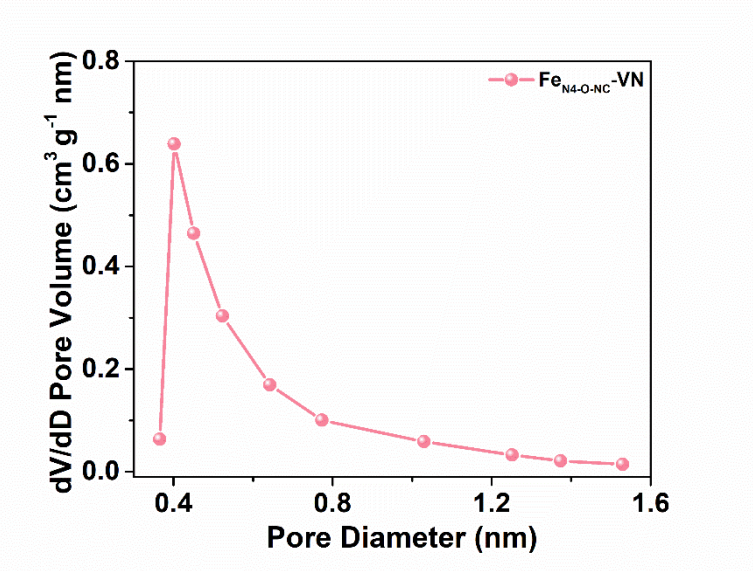

Fig. S5. The pore size distributions of $Fe_{N4-O-NC}$-VN using Horvath-Kawazoe model.

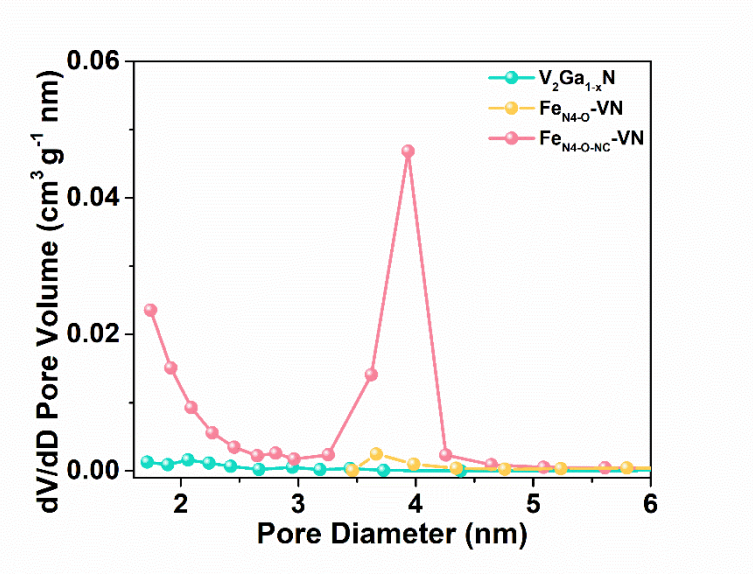

Fig. S6. The pore size distributions of $V_2Ga_{1-x}N$, Fe_{N4-O}-VN and $Fe_{N4-O-NC}$-VN using Barrett-Joiner-Halenda (BJH) model.

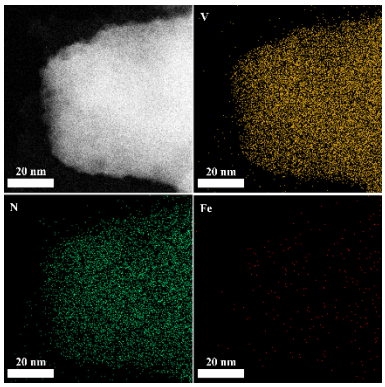

Fig. S7. TEM images and EDS mapping of Fe_{N4-O}-VN.

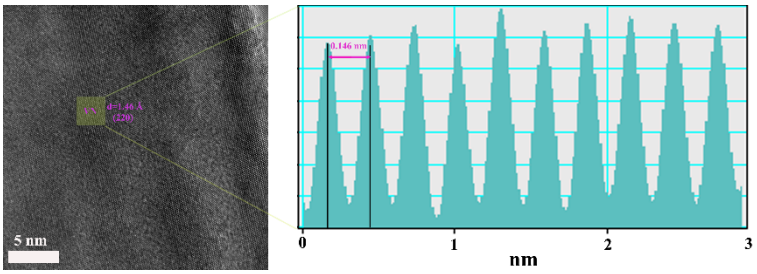

Fig. S8. TEM image and lattice distance of Fe_{N4-O}-VN.

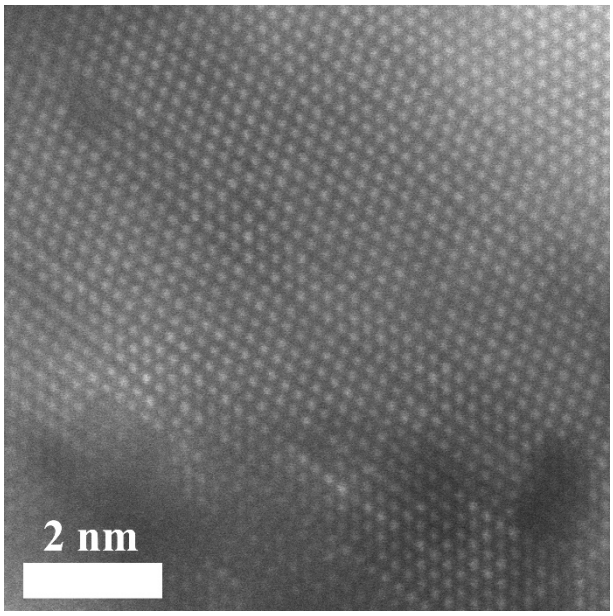

Fig. S9 HAADF-STEM image of Fe_{N4-O}-VN.

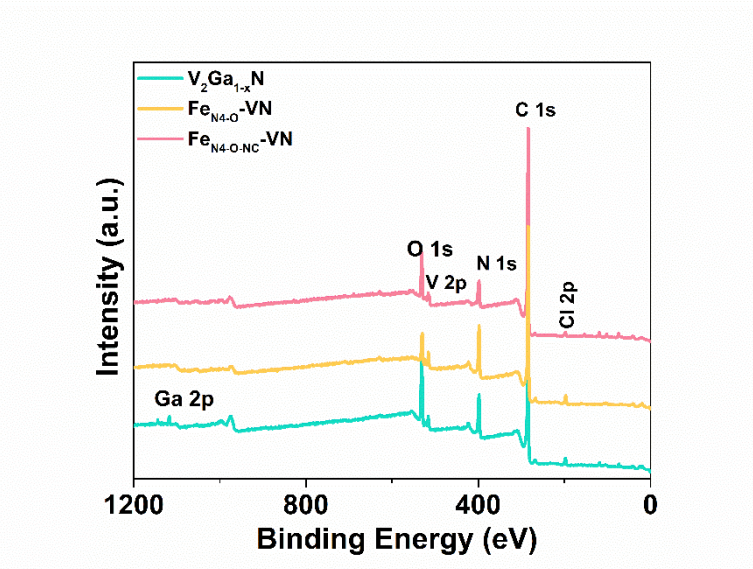

Fig. S10. The XPS survey of $V_2Ga_{1-x}N$, Fe_{N4-O}-VN and $Fe_{N4-O-NC}$-VN.

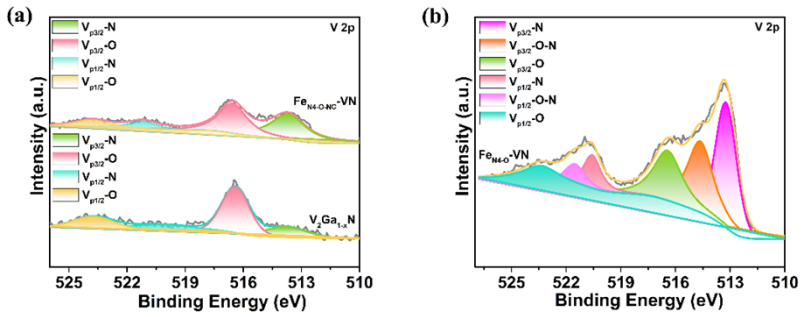

Fig. S11. High-resolution XPS spectra of V 2p in $V_2Ga_{1-x}N$, Fe_{N4-O}-VN and $Fe_{N4-O-NC}$-VN.

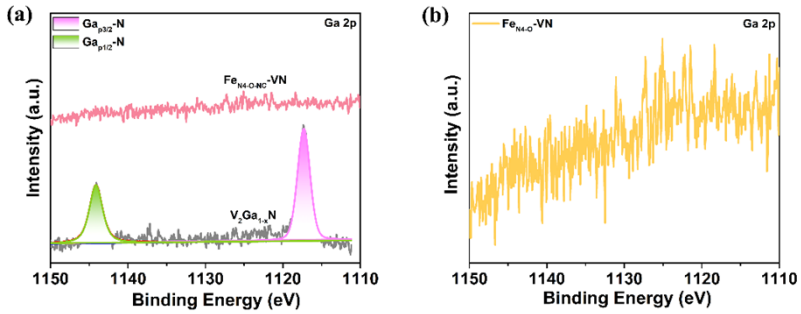

Fig. S12. High-resolution XPS spectra of Ga 2p in $V_2Ga_{1-x}N$, Fe_{N4-O}-VN and $Fe_{N4-O-NC}$-VN.

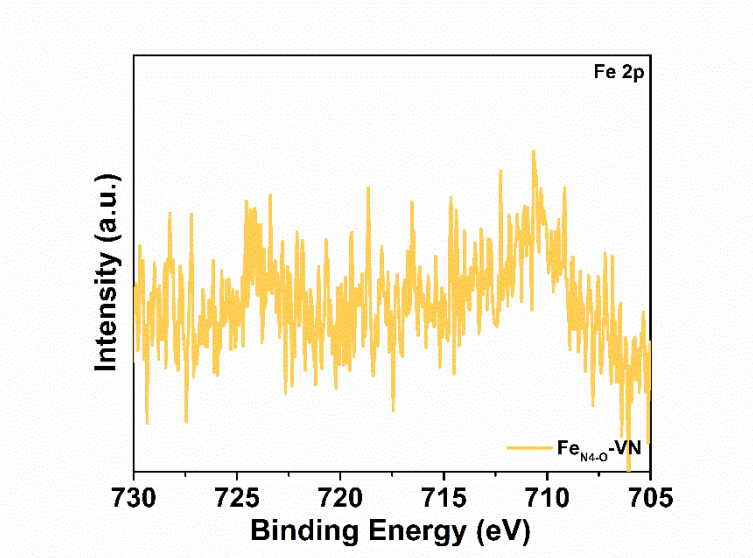

Fig. S13. High-resolution XPS spectra of Fe 2p in Fe_{N4-O}-VN.

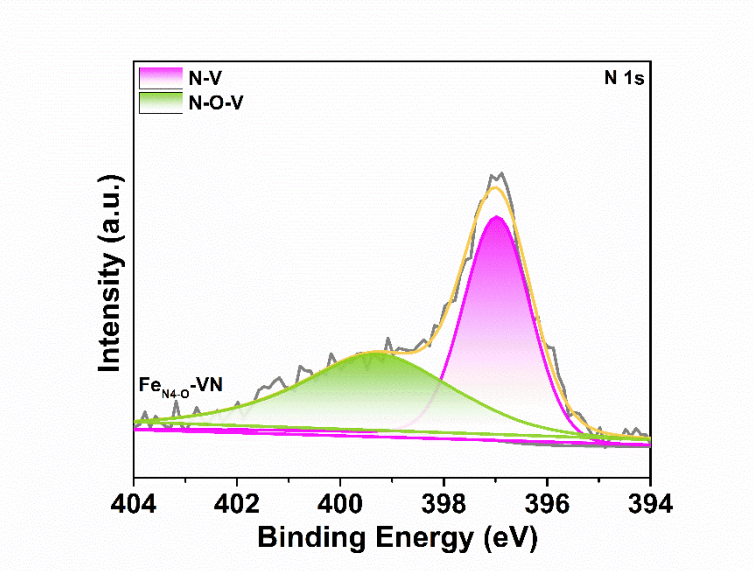

Fig. S14. High-resolution XPS spectra of Fe 2p in Fe_{N4-O}-VN.

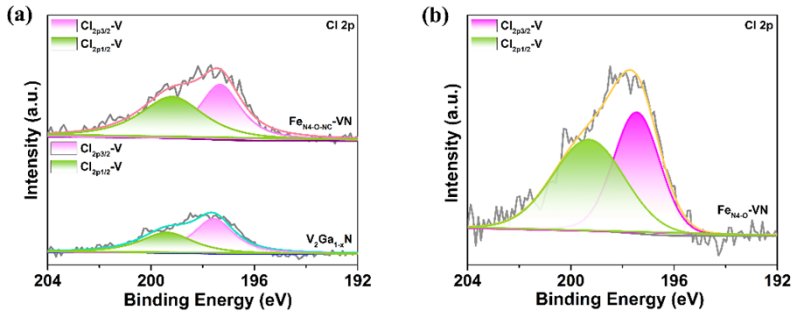

Fig. S15. High-resolution XPS spectra of Cl 2p in $V_2Ga_{1-x}N$, Fe_{N4-O}-VN and $Fe_{N4-O-NC}$-VN.

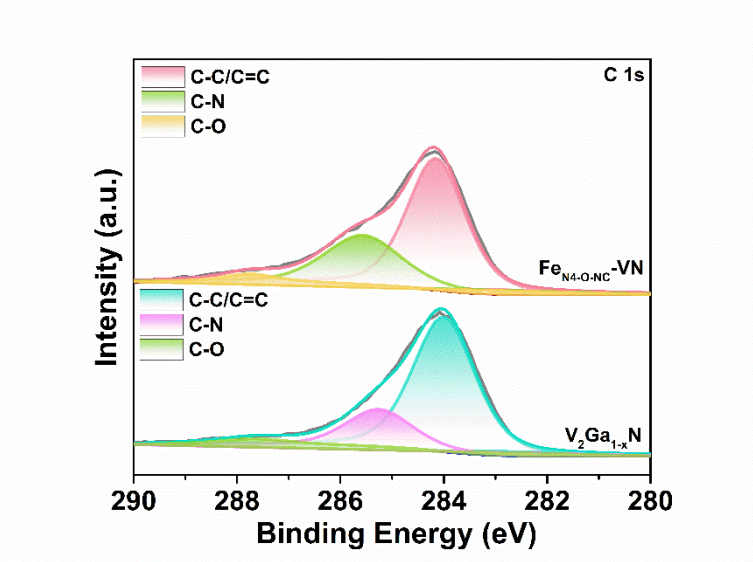

Fig. S16. High-resolution XPS spectra of C 1s in in $V_2Ga_{1-x}N$ and $Fe_{N4-O-NC}$-VN.

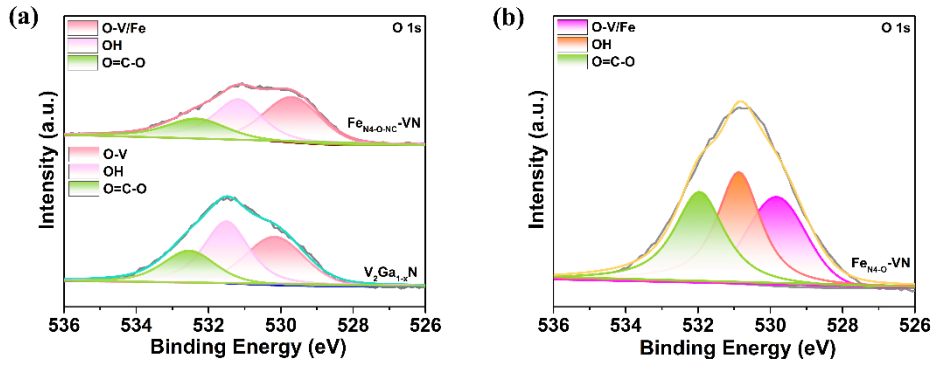

Fig. S17. High-resolution XPS spectra of O 1s in $V_2Ga_{1-x}N$, Fe_{N4-O}-VN and $Fe_{N4-O-NC}$-VN.

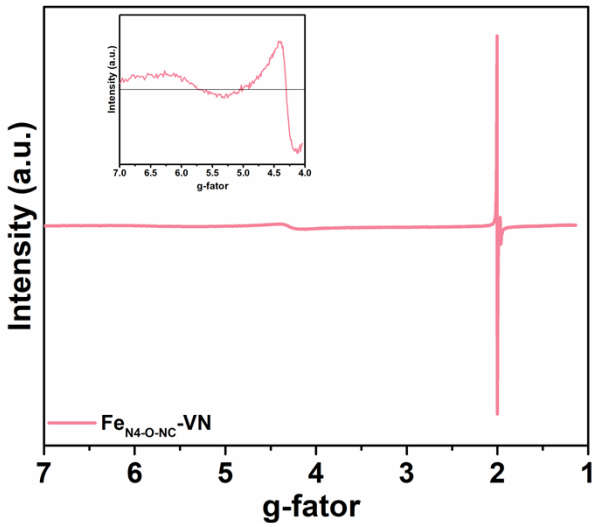

Fig. S18. EPR spectrum of $Fe_{N4-O-NC}$-VN.

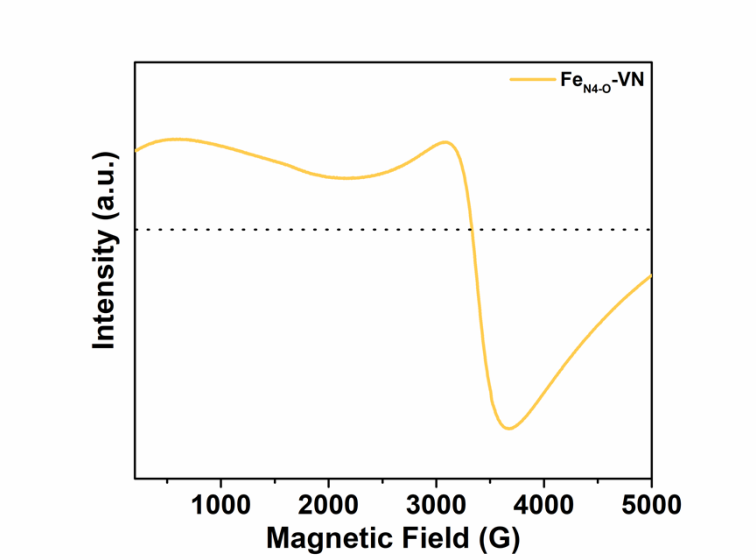

Fig. S19. EPR spectrum of Fe_{N4-O}-VN.

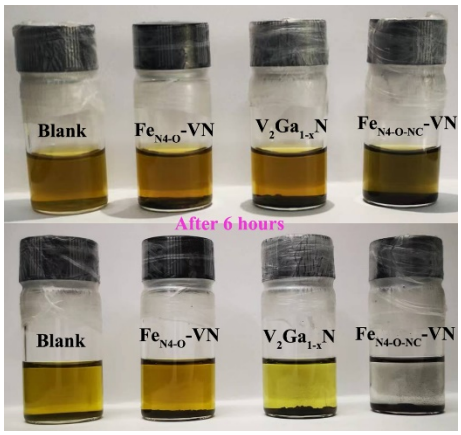

Fig. S20. Photographs of Li_2S_6 solutions before and after using different materials.

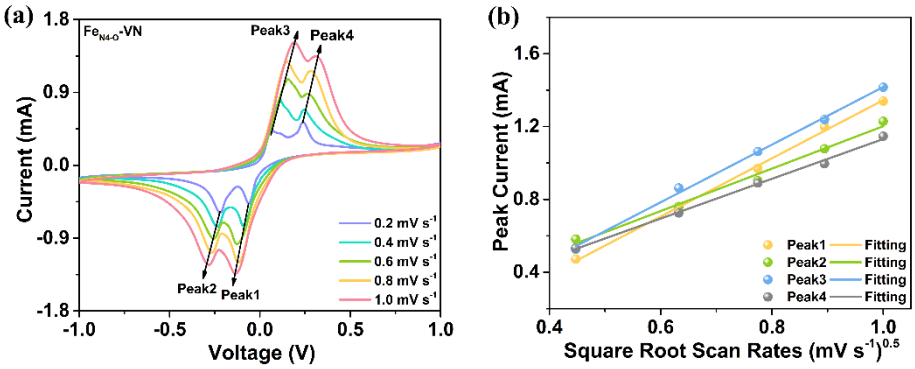

Fig. S21. CV curves of symmetric cells with Fe_{N4-O}-VN at 0.2-1.0 mV s^{-1}.

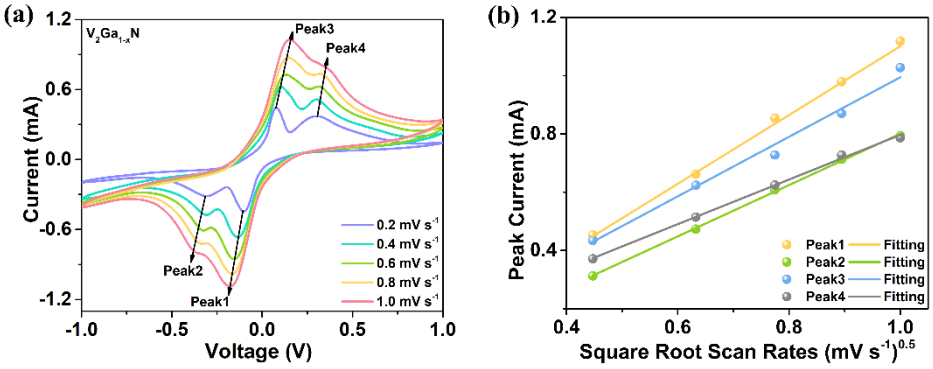

Fig. S22. CV curves of symmetric cells with $V_2Ga_{1-x}N$ at 0.2-1.0 mV s^{-1}.

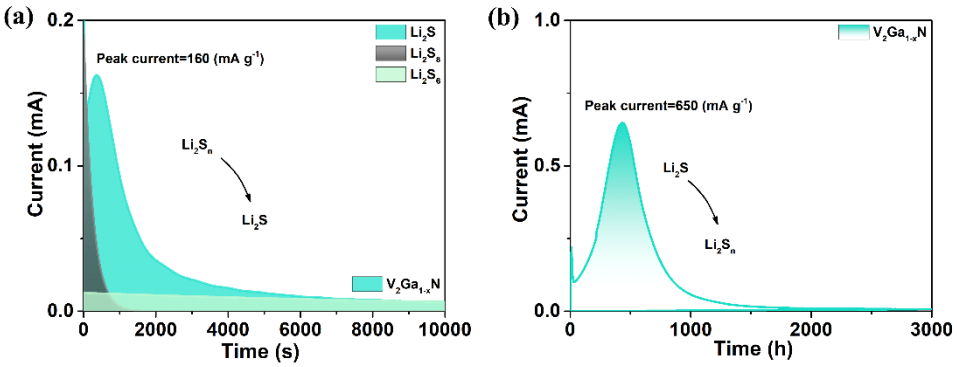

Fig. S23. (a) Precipitation and (b) dissolution plots of $V_2Ga_{1-x}N$.

Fig. S24. The permeation measurement using pristine separators in Li_2S_6 solution.

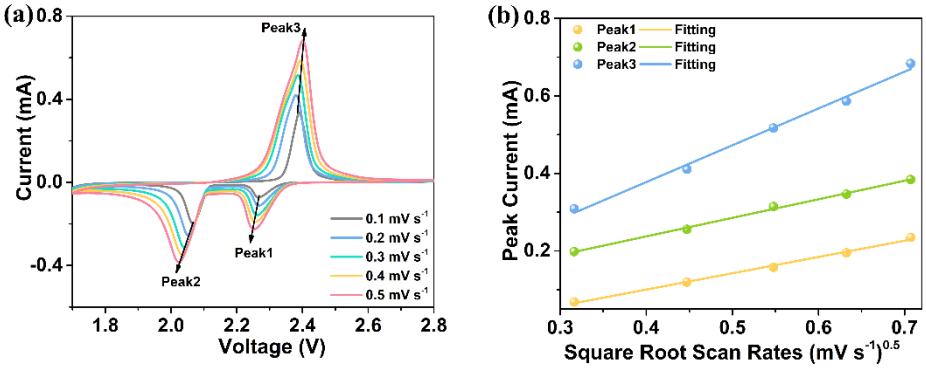

Fig. S25. (a) CV curves at 0.1-0.5 mV s^{-1}, (b) corresponding linear fitting derived from different peak currents of LSBs with Fe_{N4-O}-VN modified separator.

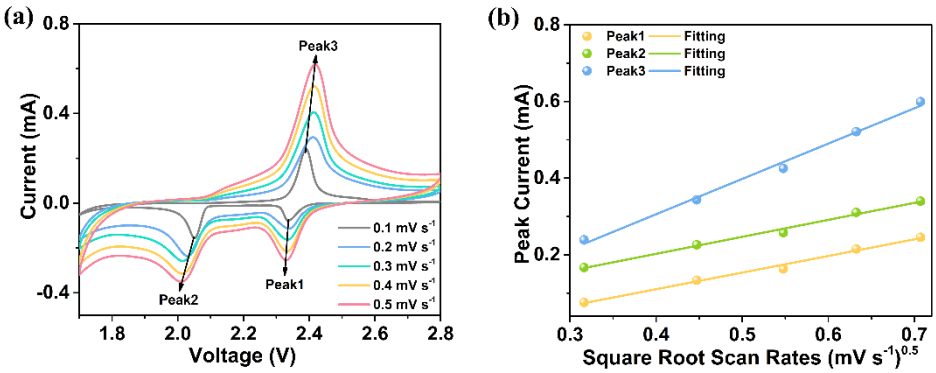

Fig. S26. (a) CV curves at 0.1-0.5 mV s^{-1}, (b) corresponding linear fitting derived from different peak currents of LSBs with $V_2Ga_{1-x}N$ modified separator.

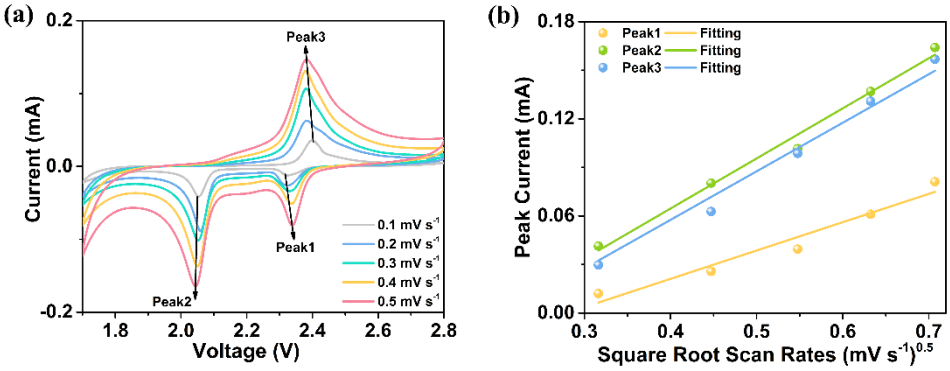

Fig. S27. (a) CV curves at 0.1-0.5 mV s^{-1}, (b) corresponding linear fitting derived from different peak currents of LSBs with pristine separator.

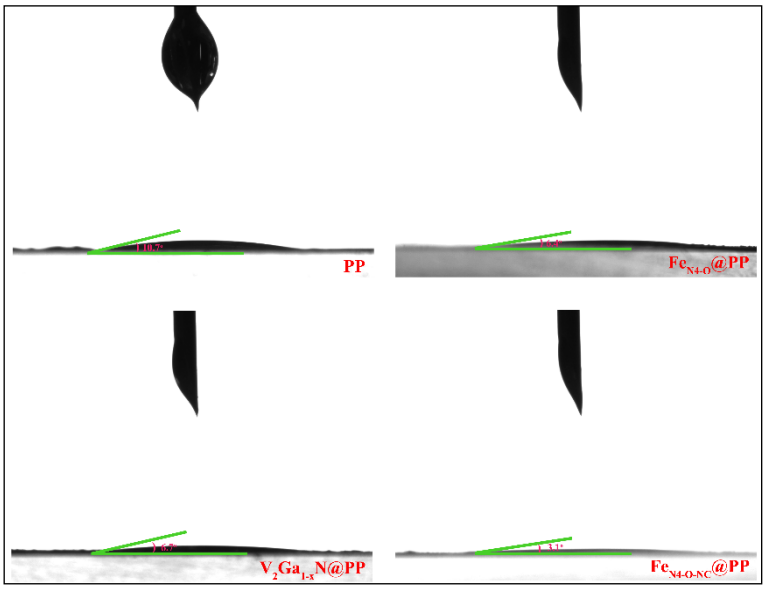

Fig. S28. Contact angle measurements of organic electrolyte on different separators.

Table S1. The specific surface areas and pore size distributions of $V_2Ga_{1-x}N$, Fe_{N4-O}-VN and $Fe_{N4-O-NC}$-VN.

Samples	BET	BJH(HK)
$V_2Ga_{1-x}N$	23.8	2.1
Fe_{N4-O}-VN	7.9	3.7
$Fe_{N4-O-NC}$-VN	377.8	3.9(0.4)

Table S2. The Fe contents determined by ICP-OES for $V_2Ga_{1-x}N$, Fe_{N4-O}-VN and $Fe_{N4-O-NC}$-VN.

Samples	Fe (wt.%)
$V_2Ga_{1-x}N$	1.06
Fe_{N4-O}-VN	1.141
$Fe_{N4-O-NC}$-VN	1.249

Table S3. The Mössbauer parameters and assignments of $Fe_{N4-O-NC}$-VN.

Component	IS (mm s^{-1})	QS (mm s^{-1})	Γ (mm s^{-1})	RA (%)	Assignment
D1	0.26	1.39	0.78	50.8	Fe, low spin
D2	0.20	3.86	0.80	38.1	Fe, intermediate spin
D3	0.31	3.05	0.37	11.1	Fe, high spin

Table S4. Comparison of electrochemical performances of the previously reported SACs modified separator or as sulfur hosts in lithium-sulfur batteries.

Samples	0.2 C (mAh g^{-1}) Initial capacity	Rate Capacity (mAh g^{-1})	Cycling Capacity (mAh g^{-1})	Cycling Number	Refs.
SA-Fe/Fe_2N@NG	1300 at 0.1 C	905 at 4 C	801.3 at 1 C	500	[7]
Pt SAs/In_2S_3/Ti_3C_2	1150	800 at 4 C	620.8 at 2 C	500	[8]
Ni-NC	1407	452 at 4 C	497 at 2 C	600	[9]
Co-O_4	1138	478 at 5 C	510 at 1 C	600	[10]
BNNs@CNFs	1244 at 0.1 C	450 at 5 C	460 at 1 C	800	[11]
W/NG	1300	900 at 5 C	605 at 2 C	1000	[12]
Cu SA/N-$Ti_3C_2T_x$	1468	925 at 3 C	801 at 2 C	400	[13]
Fe/Co-N-HPC	1456 at 0.1 C	774 at 4 C	694 at 1 C	600	[14]
SAFe@g-C_3N_4	1379 at 0.1 C	704 at 5 C	624 at 2 C	1000	[15]
N-$CoSe_2$	1341	870 at 5 C	760 at 2 C	500	[16]
SA-Zn-MXene	1136	517 at 6 C	510 at 4 C	400	[17]
SAV@NG	1230	430 at 2 C	551 at 0.5 C	400	[18]
Ni−N_5/HNPC	1188	686 at 4 C	798 at 0.5 C	500	[19]
3DFeSA-CN	1363	783 at 3 C	450 at 1 C	1000	[20]
Fe−N_3C_2−C	Nearly 1200	727.8 at 6 C	470 at 2 C	1000	[21]

Co/MoN	1570	860.6 at 1 C	554 at 1 C	500	[22]
D-MOF-Cu	1291.7	716.1 at 5 C	800 at 1 C	1000	[23]
Ni−Fe−NC	1250	580 at 4 C	700 at 1 C	600	[24]
$Fe_{N4-O-NC}$-VN	1615.7	803.7 at 5 C	857.5 at 2 C	500	This work

Table S5. The free energy of lithium polysulfides on VN, Fe_{N4-O}-VN and $Fe_{N4-O-NC}$-VN.

Samples	S_8	Li_2S_8	Li_2S_6	Li_2S_4	Li_2S_2	Li_2S
VN	0	-1.91855	-1.71781	-1.654	-1.3901	-0.49536
Fe_{N4-O}-VN	0	-2.21356	-1.95268	-1.83035	-1.66461	-0.85113
$Fe_{N4-O-NC}$-VN	0	-2.44022	-2.28708	-2.24515	-2.02401	-1.37692

Table S6. The adsorption energy of lithium polysulfides on VN, Fe_{N4-O}-VN and $Fe_{N4-O-NC}$-VN.

Samples	S_8	Li_2S_8	Li_2S_6	Li_2S_4	Li_2S_2	Li_2S
VN	-1.942	-2.004	-2.219	-2.383	2.846	2.557
Fe_{N4-O}-VN	-2.131	-2.422	-2.567	-2.919	-3.136	-2.772
$Fe_{N4-O-NC}$-VN	-2.393	-2.621	-2.947	-3.512	-3.797	-2.946

References

1. G. Kresse and J. Furthmüller, *Comp. Mater. Sci.*, 1996, **6**, 15-50.
2. G. Kresse and J. Furthmüller, *Phys. Rev. B*, 1996, **54**, 11169-11186.
3. J. P. Perdew, K. Burke and M. Ernzerhof, *Phys. Rev. Lett.*, 1996, **77**, 3865-3868.
4. G. Kresse and D. Joubert, *Phys. Rev. B*, 1999, **59**, 1758-1775.
5. P. E. Blöchl, *Phys. Rev. B*, 1994, **50**, 17953-17979.
6. V. Wang, N. Xu, J.-C. Liu, G. Tang and W.-T. Geng, *Comput. Phys. Commun.*, 2021, **267**, 108033.
7. C. Ma, Y. Zhang, Y. Feng, N. Wang, L. Zhou, C. Liang, L. Chen, Y. Lai, X. Ji, C. Yan and W. Wei, *Adv. Mater.*, 2021, **33**, 2100171.
8. C. Zhou, M. Li, N. Hu, J. Yang, H. Li, J. Yan, P. Lei, Y. Zhuang and S. Guo, *Adv. Funct. Mater.*, 2022, **32**, 2204635.
9. R. Wang, J. Qin, F. Pei, Z. Li, P. Xiao, Y. Huang, L. Yuan and D. Wang, *Adv. Funct. Mater.*, 2023, **33**, 2305991.
10. Y. Li, S. Lin, D. Wang, T. Gao, J. Song, P. Zhou, Z. Xu, Z. Yang, N. Xiao and S. Guo, *Adv. Mater.*, 2020, **32**, 1906722.
11. Y. Li, T. Gao, D. Ni, Y. Zhou, M. Yousaf, Z. Guo, J. Zhou, P. Zhou, Q. Wang and S. Guo, *Adv. Mater.*, 2021, **34**, 2107638.
12. B. X. Peng Wang, Zhengchunyu Zhang,Man Huang,Jinkui Feng,and Shenglin Xiong, *Angew. Chem. Int. Ed.*, 2021, **60**, 15563-15571.

13. H. Gu, W. Yue, J. Hu, X. Niu, H. Tang, F. Qin, Y. Li, Q. Yan, X. Liu, W. Xu, Z. Sun, Q. Liu, W. Yan, L. Zheng, Y. Wang, H. Wang, X. Li, L. Zhang, G. Xia and W. Chen, *Adv. Energy Mater.*, 2023, **13**, 2204014.
14. L. Ma, J. Qian, Y. Li, Y. Cheng, S. Wang, Z. Wang, C. Peng, K. Wu, J. Xu, I. Manke, C. Yang, P. Adelhelm and R. Chen, *Adv. Funct. Mater.*, 2022, **32**, 2208666.
15. C. Lu, Y. Chen, Y. Yang and X. Chen, *Nano Lett.*, 2020, **20**, 5522-5530.
16. M. Wang, L. Fan, X. Sun, B. Guan, B. Jiang, X. Wu, D. Tian, K. Sun, Y. Qiu, X. Yin, Y. Zhang and N. Zhang, *ACS Energy Lett.*, 2020, **5**, 3041-3050.
17. D. Zhang, S. Wang, R. Hu, J. Gu, Y. Cui, B. Li, W. Chen, C. Liu, J. Shang and S. Yang, *Adv. Funct. Mater.*, 2020, **30**, 2002471.
18. G. Zhou, S. Zhao, T. Wang, S. Z. Yang, B. Johannessen, H. Chen, C. Liu, Y. Ye, Y. Wu, Y. Peng, C. Liu, S. P. Jiang, Q. Zhang and Y. Cui, *Nano Lett.*, 2020, **20**, 1252-1261.
19. S. Zhang, X. Ao, J. Huang, B. Wei, Y. Zhai, D. Zhai, W. Deng, C. Su, D. Wang and Y. Li, *Nano Lett.*, 2021, **21**, 9691-9698.
20. Y. Ding, Q. Cheng, J. Wu, T. Yan, Z. Shi, M. Wang, D. Yang, P. Wang, L. Zhang and J. Sun, *Adv. Mater.*, 2022, **34**, 2202256.
21. G. Liu, W. Wang, P. Zeng, C. Yuan, L. Wang, H. Li, H. Zhang, X. Sun, K. Dai, J. Mao, X. Li and L. Zhang, *Nano Lett.*, 2022, **22**, 6366−6374.
22. Y. Kong, L. Wang, M. Mamoor, B. Wang, G. Qu, Z. Jing, Y. Pang, F. Wang, X. Yang, D. Wang and L. Xu, *Adv. Mater.*, 2023, 2310143.
23. Y. Xiao, S. Guo, Y. Xiang, D. Li, C. Zheng, Y. Ouyang, A. Cherevan, L. Gan, D. Eder, Q. Zhang and S. Huang, *ACS Energy Lett.*, 2023, **8**, 5107-5115.
24. J. L. Yang, P. Yang, D. Q. Cai, Z. Wang and H. J. Fan, *Nano Lett.*, 2023, **23**, 4000-4007.